OLD AND NEW PHASES IN COMPLEX LIQUIDS

D. FRENKEL

FOM Institute for Atomic and Molecular Physics [1]

1 INTRODUCTION

The subject of this lecture is computer simulation of complex liquids, such as colloids and polymeric systems. Why should computer simulation of complex liquids be any different from computer simulation of simple liquids? After all, the great charm of computer simulation is that the complexity of the computer code does not increase with the number of degrees of freedom in a system, even though the computational effort does. Indeed, the existing Molecular Dynamics simulations of polymers, micelles or proteins are not basically different from simulations of simple atomic or molecular systems. They are simply longer. Usually much longer, because one of the features that make complex liquids complex is that interesting dynamical phenomena happen over a very wide range of time scales. For instance, in polymer dynamics the characteristic decay time of the velocity of a monomer is orders of magnitude shorter than the time it takes the polymer to relax in the "tube" formed by its neighbors. And this time, in its turn, is much shorter than the time it takes the polymer to diffuse over a distance of the order of its own diameter. For atoms, the first and the third time are of the same order of magnitude.

But it is not only in their dynamics that complex liquids differ from simple liquids. Their structural properties too seem designed to make numerical simulation difficult. In particular, complex liquids may exhibit local order on at least two different length scales: namely on the scale of the atomic building blocks and on a length-scale comparable to the characteristic dimensions of the macromolecule. Finally, in order to study the phase behavior of complex liquids, we must either study phase coexistence directly using an approach based on the Gibbs-ensemble technique of Panagiotpoulos [1] or by computing the chemical potential or, more generally, the free energy ot the different phases. Such calculations are subtle for simple liquids and even more so for complex liquids.

In the present lecture, I focus on two basic topics that are of particular relevance for the simulation of complex liquids. These topics are:

(1) Kruislaan 407, 1098 SJ Amsterdam, The Netherlands.

1. Free energy calculations
2. Activated processes

I have selected these topics not only for their relevance for complex liquids, but also because they have evolved considerably over the past few years. I stress that many of the techniques that I discuss were not designed specifically for the study of complex liquids. Others were, but turn out to have interesting applications in other fields. In computer simulation, as in most areas of science, the "mobility" of techniques is quite high.

2 PHASE DIAGRAMS OF POLYMER COLLOID MIXTURES

Phase separation in binary mixtures is the example that is used in many textbooks to illustrate the competition between energy and entropy in a phase transformation. For a mixture at constant total volume V, the Helmholtz free energy F, should be minimal. As a first approximation, the entropy of mixing of a mixture of two species A and B, is replaced by the entropy of mixing of an ideal mixutre

$$S_{id}(X) = -Nk_B[X \ln X + (1 - X) \ln (1 - X)] \quad (1)$$

where X denotes the mole-fraction of one component (say A): $X = N_A/(N_A + N_B)$. The entropy of mixing given by Eq. 1 is a convex function of X. As a consequence, $S_{id}(X)$ will always decrease if phase separation takes place. This implies that phase separation can only take place if the resulting decrease in energy E outweighs the increase in $-TS_{id}$. In a hard-core mixture, there is no energy change upon mixing. Hence, if Eq. 1 were exact, we should never observe phase separation in a hard-core mixture.

The naive picture sketched above is not correct. From computer simulation [2, 3, 4, 5, 6] we know of many examples of de-mixing transitions in systems with purely hard-core interactions. Below, I discuss one particular class of de-mixing transitions in hard-core mixtures, namely depletion flocculation in colloids [7] and [8]. The reason why I discuss this example is that it allows me to introduce a technique to study phase transitions in complex fluids by computer simulation. This technique is based on an exact enumeration approach to grand-canonical simulations. In particular, we consider a mixture of two components, one of which is held at a fixed chemical potential. In some cases, we can "integrate out" the degrees of freedom of the species at fixed chemical potential.

2.1 Depletion Flocculation

Experimentally, it is well known that the addition of a small amount of free, non-adsorbing polymer to a colloidal suspension induces an effective attraction between the colloidal particles and may even lead to coagulation. This effect has been studied extensively [9] and is well understood, at least qualitatively. The polymer-induced attraction between colloids in an **entropic** effect: when the colloidal particles are close together, the total number of accessible polymer conformations is larger than when the colloidal particles are far apart. However, although the physical mechanism responsible for polymer-induced coagulation is understood **qualitatively,** a quantitative description of this phenomenon is more difficult. This is so because the polymer-induced attraction between the colloidal particles is non-pairwise additive. Moreover, it depends both on the osmotic pressure of the polymer and on the concentration of the colloid. A direct analytical evaluation of the (grand-canonical) partition function is impossible, even when one considers only the very simplest model, *viz.* that of a mixture of hard-core colloidal particles with ideal chain molecules with conformations that are restricted to a lattice. It is therefore desirable to carry out "exact" numerical simulations to investigate the phase behavior. Yet, the computational problems are still formidable. What is required is a numerical scheme that samples the positions of the colloidal particles while averaging over all possible conformations of a large (and fluctuating) number of chain molecules.

Fortunately, it is possible to construct a rigorous and efficient Monte Carlo scheme to study this model. Our approach relies on the fact that we can recursively compute the partition function of an ideal (non-self avoiding) chain on a lattice in an arbitrary external potential [7]. This is most easily seen by considering a chain of length $\ell - 1$ on lattice. Suppose that every lattice site has b neighbors, that the polymer consists of p segments and that there are N lattice sites. Clearly, for an ideal polymer in the absence of any obstacles, the total number of allowed conformations is $\Omega_{id} \equiv N \times b^p$. If obstacles are present, some random walks are blocked, and the total number of allowed conformations, Ω_T, is less than Ω_{id}. The "brute-force" method to determine the ratio Ω_T/Ω_{id} would be to attempt a large number of

insertions of chains with arbitrary conformation at random points on the lattice. The ratio of the number of "accepted" trial moves to the total number of attempted insertions can be used to compute the excess chemical potential of an ideal polymer chain in this system

$$\mu_{excess} = - k_B T \log \langle P_{acceptance} \rangle \qquad (2)$$

This is the usual "Widom" expression for the excess chemical potential [10]. However, unless the density of obstacles is quite low, the relative statistical error in the insertion probability will be quite large.

Next, consider the recursive approach. To this end, let us first compute all N Boltzmann factors associated with the insertion of a point particle at any lattice site. Clearly, the sum of these Boltzmann factors is simply the partition function of a point-particle on a lattice, in an external potential. Let us denote the Boltzmann factor associated with site i as $f_i^{(0)} \equiv \exp(- u(\mathbf{r}_i)/k_B T)$. The partition function for a one-segment polymer (2 points) is computed as follows. Starting from site i, we have b ways to grow one segment. But all b directions will, in general, have different Boltzmann weights $f_j^{(0)}$, where j denotes one of the nearest neighbors of i. The total Boltzmann weight associated with the addition of a 1-segment polymer at site i is then:

$$f_i^{(1)} \equiv f_i^{(0)} \times \left(\sum_j^b f_j^{(0)} \right) \qquad (3)$$

where the sum runs over the nearest neighbors of i. The partition function of a 1-segment polymer on a lattice is then simply:

$$\Omega_1 = \sum_{i=1}^{N} f_i^{(1)} , \qquad (4)$$

(where, for convenience, I have assumed that the polymer "head" and "tail" are distinguishable). Repeating the same argument p times, it is clear that the Boltzmann factor associated with **all possible conformations** of a p-segment polymer starting at site i is given by:

$$f_i^{(p)} = f_i^{(0)} \times \left(\sum_j^b f_j^{(p-1)} \right). \qquad (5)$$

And the total partition function is given by:

$$\Omega_p = \sum_{i=1}^{N} f_i^{(p)} . \qquad (6)$$

The important fact to note is that the computation of Ω_p, a quantity that depends on $N \times b^p$ conformations, requires only p iterations of $b \times N$ local "propagations" of real numbers. For a fixed external potential, the partition function thus computed in **exact.** In a practical situation, as with the addition of polymer to a colloidal dispersion, the external potential is not fixed, but depends on the (continuous) coordinates of all M colloidal particles, $\{\mathbf{r}^M\}$. Hence, the total partition function of the polymer also depends on these coordinates: $\Omega_p = \Omega_p(\mathbf{r}^M)$.

We now use this scheme to perform simulations of depletion flocculation. Up to this point we have not specified the nature of the "external" potential. We now assume that this potential is due to the presence of N hard, spherical colloidal particles each of which occupies many lattice sites. The polymer partition function clearly depends on the coordinates $\mathbf{r}^N$ of the colloidal particles: $\Omega_\ell(\mathbf{r}^N)$. The configurational part of the partition function of the system of N colloids plus one polymer of length ℓ in volume V is then given by:

$$Z(V, N, 1) = \int_V d\mathbf{r}^N \exp(- U_{hs}(\mathbf{r}^N)) ((\Omega_\ell(\mathbf{r}^N)), \qquad (7)$$

where $U_{hs}(\mathbf{r}^N)$ denotes the hard-sphere interaction. Next, we make use of the fact that we are considering **ideal** polymers. In that case we can immediately write down the corresponding partition function for N colloids and M ideal polymers:

$$Z(V, N, M) = \int_V d\mathbf{r}^N \exp(- U_{hs}(\mathbf{r}^N) (\Omega_\ell(\mathbf{r}^N))^M / M!, \qquad (8)$$

where the factor $1/M!$ accounts for the fact that the polymers are indistinguishable. Using Eq. 8 it is straightforward to transform to an ensemble where the polymer chemical potentiel (i.e. the osmotic pressure) is kept fixed. The corresponding grand-canonical partition function is given by:

$$\Xi(V, N, \mu) = \sum_{M=0}^{\infty} \exp(M \mu_{ch}) Z(V, N, M)/M!$$

$$= \int_V d\mathbf{r}^N \exp(-U_{hs}(\mathbf{r}^N)) \sum_{M=0}^{\infty} \exp(M \mu_{ch}) (\Omega_\ell(\mathbf{r}^N))^M / M!$$

$$= \int_V d\mathbf{r}^N \exp(-U_{hs}(\mathbf{r}^N)) \exp(z\Omega_\ell(\mathbf{r}^N)) \qquad (9)$$

In the last line of Eq. 9, we have introduced the polymer activity $z \equiv \exp(\mu_{ch})$, where μ_{ch} denotes the chemical potential of the chain molecules.

The important point to note is that Eq. 9 allows us to evaluate the properties of the colloidal particles in osmotic equilibrium with a polymer reservoir. In particular, it shows that we can perform Monte Carlo sampling of the colloidal particles. The polymers only affect $U_{eff}(\mathbf{r}^N)$, the effective interaction between the colloidal particles:

$$U_{eff}(\mathbf{r}^N) \equiv U_{hs}(\mathbf{r}^N) - z\Omega_\ell(\mathbf{r}^N). \qquad (10)$$

$z\Omega_\ell(\mathbf{r}^N)$ measures the entropic interaction between the colloids due to **all** possible polymer conformations. This entropic interaction is, in principle, not pairwise additive. In fact, it is shown in Ref. [8], that for all but the shortest chain molecules, this non-additivity of the polymer-induced interaction between the colloids, has a pronounced effect on the structure and stability of the mixture. For more details, we refer the reader to Ref. [8].

Whether a given compound will have a liquid phase, depends sensitively on the range of the intermolecular potential: as this range is decreased, the critical temperature approaches the triple-point temperature, and when T_c drops below the latter, only a single stable fluid phase remains. This phenomenon is well known in mixtures of spherical colloidal particles and non-adsorbing polymer, where the range of the attractive part of the effective colloid-colloid interaction can be varied by changing the size of the polymer [11, 12, 13, 7, 8]. Experiment, theory and simulation all suggest that when the width of the attractive well becomes less than approximately one third of the diameter of the colloidal spheres, the colloidal "liquid" phase disappears.

Consider, for instance, the phase behavior of an a hard-core fluid with an attractive Yukawa interaction:

$$u(r) = \begin{cases} \infty & (r < \sigma) \\ -\varepsilon \dfrac{\exp(\kappa\sigma(1 - r/\sigma))}{r/\sigma} & (r \geq \sigma) \end{cases} \qquad (11)$$

where σ is the diameter of the hard core, ε is the well depth, and κ^{-1} is a measure for the range of the attractive part of the potential.

Computer simulations [14] show that, if the range of the attraction is larger than approximately 20% of the hard-core diameter, a liquid-vapor transition is possible. For example, Fig. 1 shows the results of a computer simulation of a Yukawa system with $\kappa\sigma$ = 3.9. In this case, liquid-vapor coexistence is clearly present. In contrast, when $\kappa\sigma$ = 7 (see Fig. 2). The liquid-

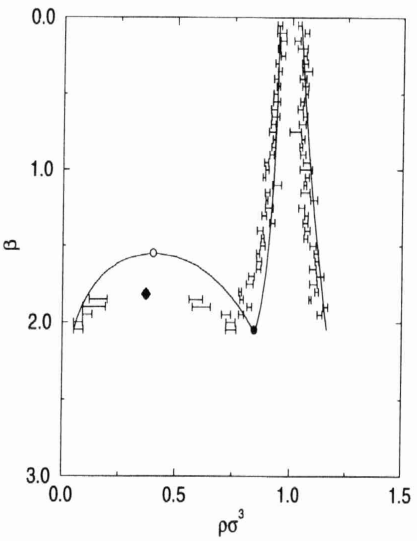

Figure 1

Phase diagram of the hard-core attractive Yukawa system (see Eq. 11) for $\kappa\sigma$ = 3.9. In this figure the open circle denotes the critical point, the filled circle the triple point and the drawn lines correspond to the results of first order perturbation theory (see Ref. [14]). The points with error-bars are the simulation results. The diamond indicates the critical point as obtained by Gibbs-ensemble simulations.

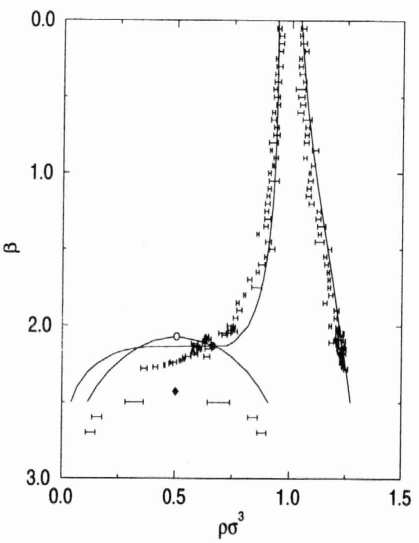

Figure 2

Phase diagram of the hard-core attractive Yukawa system (see Eq. 11) for $\kappa\sigma$ = 7. In this figure the open circle denotes the critical point, the filled circle the triple point and the drawn lines correspond to the results of first order perturbation theory (see Ref. [14]). The points with error-bars are the simulation results. The diamond indicates the metastable critical point as obtained by Gibbs-ensemble simulations.

vapor coexistence curve has moved below the sublimation line, indicating the absence of a stable liquid range. In fact, there is even numerical evidence that in a molecular compound (C_{60}), the range of the intermolecular attraction may be sufficiently short to suppress the liquid-vapor transition [15]. Next, consider what happens in systems with a very short ranged attraction, where the liquid-vapor transition is absent. Such systems could be realized in mixtures of uncharged colloids and short polymers. Recent computer simulations [16] and [17] show that such systems may exhibit a solid-solid transition that is in many ways reminiscent of the liquid-vapor transition: in particular,

1. The transition takes place between two phases that have the **same** structure
2. The line of (first-order) solid-solid transitions ends in a critical point, and
3. The transition depends strongly on the range of the intermolecular attraction

As a first approximation, we use the square well potential to model short-ranged interactions in mixtures of uncharged colloids and polymers. The square-well model potential is harshly repulsive at distances less than a characteristic diameter σ and has an attractive interaction with a characteristic range δ, outside the repulsive core. The functional form of the square-well potential is:

$$v(r) = \begin{cases} \infty & 0 \le r < \sigma \\ -\varepsilon & \sigma \le r < \sigma + \delta \\ 0 & r \ge \sigma + \delta \end{cases}, \qquad (12)$$

where ε is the depth of the attractive well. In fact, the occurrence of the solid-solid transition in systems with short ranged potentials is not sensitive to the precise form of the potential and is therefore likely to be experimentally observable. Additional evidence for the insensitivity of the solid-solid transition to the precise shape of the intermolecular potential comes from recent theoretical work by Tejero et al. [18] and the simulations of ref. [17].

It is well known that systems with a short-ranged attraction cannot exhibit a phase transition in one dimension. However, our simulations show that such a transition is possible in two dimensions. As will be discussed below, this turns out to have interesting consequences. In order to compute the phase diagram of the square-well system, we first must determine the dependence of the Helmholtz free energy of the solid on density and temperature. As the free energy of the solid

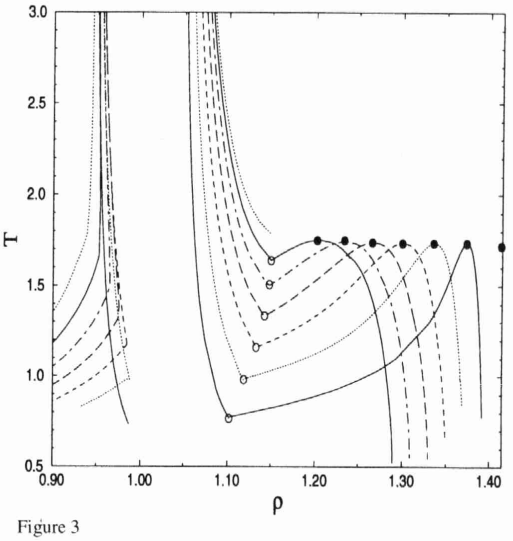

Figure 3

Simulated T, ρ phase diagrams for the fcc structure of hard spheres with an attractive interaction (square well) with range δ. Starting with the coexistence curve on the right, from right to left the curves correspond to the well widths δ/σ = 0.01, 0.02, 0.03, 0.04, 0.05 and 0.06. The upper dashed fluid-solid coexistence curve refers to a well width of δ/σ = 0.07 and shows that the solid-solid transition has become meta-stable at this point. The critical points are indicated by filled circles, the triple points by open circles.

cannot be measured directly in a Monte Carlo simulation, we use thermodynamic integration to relate the free energy of the square-well solid to that of a reference hard-sphere solid at the same density [19].

In order to map out the phase diagram of the square-well solid over a wide range of densities and temperatures as a function of the width of the attractive well, several thousand independent simulations were required. To keep the computational costs within bounds, we chose to simulate a relatively small system. With a small system size, finite-size effects are expected, in particular in the vicinity of a critical point. However, away from critical points finite-size effects should be so small that they will not affect the conclusions that we draw below.

In what follows, we use reduced units, such that ε/k_B is the unit of temperature, and σ, the hard-core diameter of the particles, is the unit of length. Fig. 3 shows the computed solid-solid and fluid-solid coexistence curves in the ρ, T plane for the two and three dimensional square-well models. We first focus on the solid-solid transition. The density gap between the dense and expanded *fcc* solids is wide at low temperatures and shrinks to zero when the solid-solid critical point is ap-

proached. Because of the analogy with liquid-vapor coexistence, one would expect that the solid-solid critical point should be of the 2D and 3D-Ising universality class.

The coexistence curves are asymmetric, especially in the limit $\delta \rightarrow 0$. In this limit, the reduced critical temperature T_c goes to a finite limiting value of approximately 1.7 in three dimensions and 0.92 in two. This may seem surprising but, in fact, this limit can be studied directly using a peculiar lattice model [17].

The solid-solid coexistence region shifts to lower densities as the well-width is increased. This effect can easily be understood by noting that a dense square-well solid can be expanded at virtually no cost in potential energy, up to the point where the nearest-neighbor separation is $\sigma + \delta$. It is only when the solid is expanded beyond this limit that the potential energy increases steeply and a transition to the expanded solid may occur. Hence, the larger δ, the lower the density where the phase transition will take place. When δ becomes larger, the vapor-solid-solid triple point shifts to higher temperatures and densities, until it reaches the critical temperature. At that point the solid-solid transition disappears because for larger values of δ it is pre-empted by the melting transition. This happens when $\delta > 0.06$. It should be noted that iso-structural solid-solid transitions are known to occur in dense *Cs* and *Ce* [20]. However, in this case the intermolecular potential is too long ranged to induce the mechanism described above and the transition is believed to be due to the **softness** of the intermolecular potential associated with a pressure-induced change in the electronic state of the metal ions.

3 CRYSTAL NUCLEATION

Crystal nucleation is a prototypical example of an activated process. In classical nucleation theory, the free energy barrier that separates the supercooled fluid from the stable solid is estimated, assuming that crystallization proceeds through the formation of essentially spherical crystal nuclei. The reason why a barrier developed is that to lowest order, the free energy of such a nucleus contains two terms, a negative "bulk" term, proportional to the cube power of the radius r of the nucleus, and a positive "surface" term, proportional to the square of the radius.

$$\Delta F_{cl} = \frac{4\pi}{3} r^3 \rho \Delta\mu + 4\pi r^2 \gamma , \qquad (13)$$

where ρ is the number density of the nucleus, $\Delta\mu$ is the difference in chemical potential of the solid and the liquid ($\Delta\mu < 0$ for super-cooled liquids) and γ is the solid-liquid interfacial free energy. The top of the free energy barrier is obtained as the maximum of ΔF_{cl} in Eq. 13. It is easy to see that the barrier height scales as $\gamma^3/\Delta\mu^2$. At coexistence, $\Delta\mu = 0$ and hence the nucleation barrier is infinite. Clearly, we need a substantial amount of super-cooling, before spontaneous crystallization will occur. To give a rough estimate: experimentally, crystal nucleation becomes observable if the number of nuclei that are formed per second per cubic centimeter is of the order of one. This will happen typically if the fluid is super-cooled by 10-15%. Now let us assume that we wish to study this phenomenon by simulation. Then we are forced to study much smaller systems. Let us assume that we perform a really large simulation, involving millions of particles. Even then, our simulation box has a volume less that 10^{-15} cm^3. And hence if we wish to observe a nucleation event with a rate of 1 s^{-1}cm^{-3}, we will, on average have to wait for 10^{15} seconds before a nucleus forms in a simulation box. The computer time involved easily exceeds the lifetime of the universe by orders of magnitude.

It is for this reason that most computer simulations of crystal nucleation have been performed under conditions of extreme super-cooling, where the nucleation rate is 20-30 orders of magnitude higher. This involves supercooling the fluid to a temperature some 50% below the freezing point. The problem is that such extreme super-coolings are quite unrealistic. The way crystallization proceeds under those conditions can differ not just quantitatively, but even qualitatively from what happens at moderate super-cooling – the crystal phase that forms on nucleation may be different. This is particularly obvious if, at low temperatures, another crystal structure is more stable than close to melting. But even if the stable structure is the same, the phase that nucleates may still be different. This was already recognized in 1897 when Ostwald [21] formulated his famous "step" rule, which states that the crystal phase that is nucleated from the melt need not be the one that is thermodynamically most stable, but the one that is closest in free energy to the fluid phase. Stranski and Totomanow [22] reexamined this rule and argued that the phase that will form is the one that has the lowest free-energy barrier of formation, rather than the phase that is globally stable under the conditions prevailing. Clearly, the relative height of such free energy barriers may change as the fluid is more and more

strongly super-cooled. To give a specific example, let us consider crystallization of a simple liquid, such as a liquid noble gas. Such liquids can easily be studied by computer simulation. The interaction between noble gas atoms is well represented by the Lennard-Jones potential. And hence a study of crystallization in the Lennard-Jones system provides us with insight into the freezing mechanism for simple liquids. In the late seventies, Alexander and McTague [23] argued, on the basis of theoretical arguments that, at least for small super-cooling, nucleation of the body-centered cubic (bcc) phase should uniquely be favored in all simple fluids exhibiting a weak first order phase transition. However, when attempts were made to investigate the formation of meta-stable bcc nuclei on a microscopic scale, using computer simulation [24, 25, 26, 27, 28, 29, 30], the picture that emerged gave little support for the Alexander-McTague scenario. For the Lennard-Jones system, which is known to have a stable face-centered cubic (fcc) structure up to the melting curve, the formation of a meta-stable bcc phase was observed in only one of the simulation studies reported [24], while all other studies [25, 26, 27, 28, 29, 30] found evidence for the formation of fcc nuclei. Of particular interest is the simulation of Swope and Andersen [30] on a system comprising one million (!) Lennard-Jones particles. This study showed that, although both fcc and bcc nuclei are formed in the early stages of the nucleation, only the fcc nuclei grow into larger crystallites. It should be noted however, that in all these simulation studies, very large degrees of super-cooling (down to 50 % of the melting temperature, or lower) had to be imposed to see any crystal formation on the time-scale of the simulation. As argued above, for such a large super-cooling one should expect the free-energy barrier for nucleation into essentially all possible crystal phases to be quite small. It is therefore not obvious that crystal nucleation at large super-cooling will proceed in the same way as close to the freezing point.

An alternative approach to the study of crystal nucleation (and activated events in general) is not to simply wait for the rare event to happen, but to directly measure the free energy barrier and the crossing rate, using a combination of numerical techniques [31, 32, 33, 34, 35].

As an example, consider homogeneous nucleation in a Lennard-Jones system close to the freezing point. Rather than using a "brute-force" approach where we wait for nuclei to form spontaneously, we use the scheme [35] to study the free-energy barrier to crystal nucleation. The advantage of this technique is that it can be used even at small (i.e. realistic) super-cooling where the straightforward molecular dynamics technique will not work, because the nucleation barrier diverges at coexistence. Moreover, the sampling technique that we employ [35, 36] allows us to stabilize the critical nucleus and study its structure in detail.

In order to measure the free-energy barrier that separates the super-cooled liquid from the solid, we must first define an order parameter which acts as a "reaction coordinate", in the sense that it has a small value in the liquid state and a large value when the system has crystallized. Moreover, as we do not know *a priori* which crystal structure will form, we must use an order parameter that is only sensitive to the overall degree of crystallinity in the system but not to the differences between the possible crystal structures. Van Duijneveldt and Frenkel [35] have shown that the bond orientational order parameter Q_6 (see below), first introduced by Steinhardt, Nelson and Ronchetti [37], satisfies these requirements and can be conveniently implemented in numerical simulations.

The Gibbs free energy of the system, G, is a function of this order parameter [38]:

$$G(Q_6) = \text{constant} - k_B T \ln [P(Q_6)], \qquad (14)$$

where $P(Q_6)$ is the probability per unit interval to find the order parameter around a given value of Q_6. Both Monte Carlo (MC) and Molecular Dynamics (MD) simulations were performed to measure $P(Q_6)$. In order to get a reliable estimate of $P(Q_6)$ even near the top of the barrier, we used the so-called "umbrella sampling" technique of Torrie and Valleau [36], in which the sampling of configuration space is biased in such a way that good statistics can be obtained even near the top of the barrier.

The simulations were carried out at constant temperature and pressure. In what follows we use reduced units, such that the Lennard-Jones well-depth ε is the unit of energy, while the Lennard-Jones diameter σ is the unit of length. In order to minimize artifacts due to the finite system size, we simulated a fairly large system, i.e. of 10648 particles. Simulations were performed both in the direction of increasing and decreasing crystallinity. All results reported below are based on simulations that were free of hysteresis. It should be stressed, however, that, near the top of the barrier, very

long simulations were required to equilibrate the system.

In our simulations, we studied the nucleation barrier under conditions of moderate (20%) super-cooling, at two different pressures: $P = 0.67$ ($T = 0.6$) and $P = 5.68$ ($T = 0.92$). We find that initially, as Q_6 is increased from the liquid, the number of small solid clusters in the liquid increases. The reason why there are, initially, several small solid clusters is that it is entropically favorable for the system to distribute a given amount of crystallinity over several clusters. However, as the top of the barrier is approached, the energetic factors dominate and several of these small solid clusters combine into a large one. This cluster corresponds to the critical nucleus. When Q_6 is increased even further this critical nucleus grows. Fig. 4 shows the Gibbs free energy of the system relative to the liquid phase, as a function of crystallinity (Q_6). The value of the Gibbs free energy of the system at the top of the barrier corresponds to the nucleation barrier. We have compared the measured nucleation barrier with the corresponding prediction of classical nucleation theory.

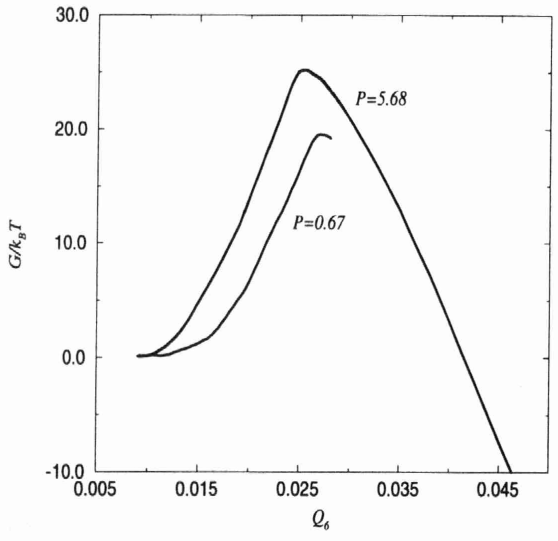

Figure 4

Gibbs free energy of a Lennard-Jones system as a function of crystallinity (Q_6) at 20% under-cooling for two different pressures, i.e. $P = 5.68$ ($T = 0.92$) and $P = 0.67$ ($T = 0.6$). The Gibbs free-energy barriers are approximately 25.1 k_BT at $P = 5.68$ and 19.4k_BT at $P = 0.67$.

This theory yields the following predictions for the nucleation barriers: $G/k_BT = 17.4$ at $P = 0.67$ and $G/k_BT = 8.2$ at $P = 5.68$. We find from our simulations that $G/k_BT \approx 19.4$ for the lower pressure (see Fig. 4), which is in good agreement with the theoretical prediction. The discrepancy between CNT and simulation for $P = 5.68$ is most likely mainly due to the fact that the the solid-liquid interfacial free energy under these conditions is not known accurately.

Next, we consider the structure of the crystal nuclei. In order to analyse the structure of a crystalline cluster, we first determine which particles are "solid-like". This is largely a technical problem that I will not discuss here [39]. Once we have identified the "solid-like" clusters, we wish to characterize the local crystal structure of the clusters. We found it most convenient to compare the local structure of the nucleus to three limiting cases: liquid, fcc-crystal and bcc-crystal. In practice, we attribute to every structure a certain fraction f_{liq} of "liquid" character, while f_{fcc} and f_{bcc} measure the fraction of fcc and bcc character. Finally, as no structure can be perfectly decomposed into these three components, we also measure the quality of the fit by determining the "mismatch" Δ. If $\Delta = 0$, the structure behaves as a linear superposition of liquid, fcc and bcc structures. If Δ is large, no linear combination of these structure provides a good description of our nucleus. To give a specific example, if we were to apply our analysis to a thermally equilibrated fcc crystal, we would find $f_{fcc} = 1$ and $\Delta = 0$.

With the technique described above, we can analyse the structure of the nuclei that form in the super-cooled Lennard-Jones fluid. Fig. 5 shows f_{liq}, f_{bcc} and f_{fcc} for the largest cluster in our system as the system moves up the nucleation barrier (for $P = 5.68$). We note that the pre-critical nuclei are predominantly bcc-like with an appreciable "liquid-like" character. However, near the top of the barrier there is a clear change in the nature of the solid nuclei from bcc-like to fcc-like. The fact that the pre-critical nuclei are rather liquid-like is not very surprising as they are very small and almost all interface. What is more interesting is that these nuclei are clearly more bcc ordered than fcc ordered. This suggests that, at least for small crystallites, we find the behavior predicted by the Alexander-McTague theory [23]. Yet, as the larger clusters are increasingly fcc-like, the present results are also compatible with the findings

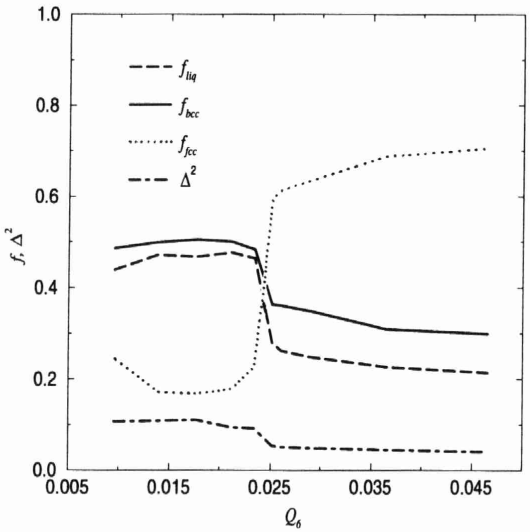

Figure 5

Structural composition of the largest cluster, indicated by f_{liq}, f_{bcc}, f_{fcc} and Δ^2, as a function of Q_6 at 20% super-cooling (P = 5.68, T = 0.92). This figure is based on averages over 50 independent atomic configurations.

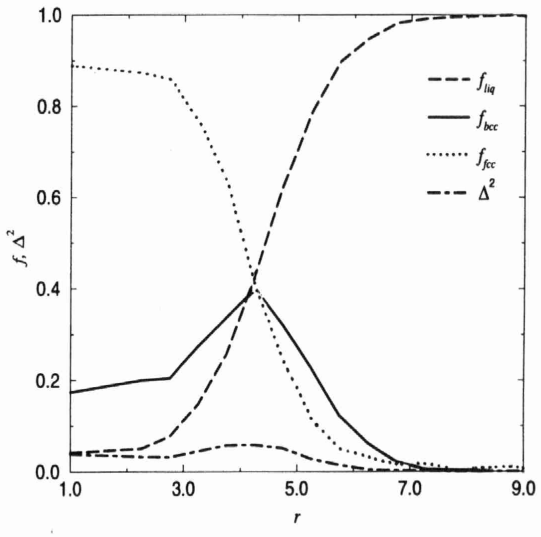

Figure 6

Structure of the critical nucleus, indicated by f_{liq}, f_{bcc}, f_{fcc} and Δ^2, as a function of r, the distance to its center-of-mass, at 20% super-cooling (P = 5.68, T = 0.92). This figure is based on averages over 50 independent atomic configurations.

of Swope and Andersen [30], who observed that nucleation proceeded through fcc crystallites.

Still, we note that the critical and post-critical nuclei are not fully fcc ordered. They have both appreciable liquid-like and bcc-like character. It is not surprising to find some liquid-like behavior as the nuclei still have a relatively large crystal-liquid interface. But the bcc-like character is more intriguing. To show what is at the cause of this behavior, we have analysed the **local** order of the critical nucleus. We calculate f_{liq}, f_{bcc} and f_{fcc} in a spherical shell of radius r around the center-of-mass of the cluster. Fig. 6 shows the radial profile of the local order of the critical nucleus. As expected, we find that the core of the nucleus is predominantly fcc-like and that f_{liq} and f_{fcc} smoothly go to one and zero, respectively, in the liquid. Surprisingly, f_{bcc}, before decaying to zero in the liquid, increases at the interface and becomes even larger than f_{fcc}. The surface enhancement of the bcc signature is absent when we bring a fcc crystallite in contact with a liquid and do not allow the surface structure to relax. Hence, the present simulations suggest that the fcc-like core of the equilibrated nuclei is "wetted" by a shell which has more bcc character. This also explains the overall bcc character of the pre-critical nuclei: the structure of these small clusters is almost completely surface dominated.

This example illustrates that, with suitable simulation techniques, it is possible to study the rate limiting step of activated processes in great detail. This would not have been possible with "brute force" simulations. Using the present scheme, it is also possible to arrive at quantitative predictions of nucleation rates, even in the regime where crystal nucleation is very slow.

It should be emphasized that the present example of crystallization in a Lennard-Jones system is simply meant as an illustration. The technique is, in no way, limited to such simple systems and, in fact, the most interesting applications lie, no doubt, in the study of homogeneous and heterogeneous nucleation (or the suppression thereof) in complex liquids.

The work of the *FOM Institute* is part of the research program of *FOM* and is supported financially by the *Netherlands Organization for Research (NWO).*

REFERENCES

1 See the contribution of B. Smit, elsewhere in this volume, and B. Smit in M.P. Allen and D.J. Tildesley, Eds. (1993), *Computer Simulation in Chemical Physics,* pages 461-472. Kluwer, Dordrecht.

2 Dijkstra M and D. Frenkel (1994). *Phys. Rev. Lett.*, **7**, 2298-300.

3 Dijkstra, D. Frenkel and J.-P. Hansen (1994). *J. Chem. Phys.*, **101,** 3179.

4 van Duijneveldt J.S. and H.N.W. Lekkerkerker (1993). *Phys. Rev. Lett.*, **71**, 4264-4266.

5 Bolhuis P.G. and D. Frenkel (1994). *J. Chem. Phys.*, **101,** 9869-9875.

6 Kranendonk W.G.T. and D. Frenkel (1991). *Mol. Phys.*, **72,** 679.

7 Meijer E.J. and D. Frenkel (1991). *Phys. Rev. Lett.*, **67,** 1110.

8 Meijer E.J. and D. Frenkel (1994). *J. Chem. Phys.*, **100,** 6873-6887.

9 Napper D.H. (1983), *Polymeric Stabilization of Colloidal Dispersions.* Academic Press.

10 Widom B. (1963). *J. Chem. Phys.*, **39,** 2808.

11 Gast A.P., C.K. Hall, and W.B. Russel (1983). *J. Coll. Interf. Sci.*, **96,** 251.

12 Asakura S. and F. Oosawa (1958). *J. Pol. Sci.*, **33,** 183.

13 Pusey P.N., in *Liquids, freezing and glass transition,* J.P. Hansen, D. Levesque, and J. Zinn-Justin (Eds.) (1991). North-Holland, Amsterdam, p. 763.

14 Hagen M.H.J. and D. Frenkel (1994). *J. Chem. Phys.*, **101,** 4093.

15 Hagen M.H.J., E.J. Meijer, G.C.A.M. Mooij, D. Frenkel, and H.N.W. Lekkerkerker (1993). *Nature,* **365,** 425.

16 Bolhuis P. and D. Frenkel (1994). *Phys. Rev. Lett.*, **72,** 2211.

17 Bolhuis P.G., M.H.J. Hagen and D. Frenkel (1994). *Phys. Rev. E,* ***50,*** 4880-4890.

18 Tejero C.F., A. Daanoun, H.N.W. Lekkerkerker, and M. Baus (1994). *Phys. Rev. Lett.*, **73,** 752 (see also: A. Daanoun, C.F. Tejero, and M. Baus (1994) *Phys. Rev. E,* **50,** 2913; C.N. Likos, Zs. T. Németh, and H. Löwen (1994). *J. Phys. Condensed Matter,* **6,** 10965.

19 Frenkel D. in *Molecular Dynamics Simulation of Statistical Mechanical Systems,* G. Ciccotti and W.G. Hoover (Eds.) (1986). North-Holland, Amsterdam, p. 151.

20 Jayaraman A., (1965), *Phys. Rev.,* **137,** A179.

21 Ostwald W. (1897). *Z. Phys. Chem.*, **22,** 289.

22 Stranski I.N. and D. Totomanow (1933). *Z. Physikal. Chem.*, **163,** 399.

23 Alexander S. and J.P. McTague (1978). *Phys. Rev. Lett.*, **41,** 702.

24 Mandell M.J., J.P. McTague, and A. Rahman (1977). *J. Chem. Phys.*, **66,** 3070.

25 Mandell M.J., J.P. McTague, and A. Rahman (1976). *J. Chem. Phys.*, **64,** 3699.

26 Hsu C.S. and A. Rahman (1979). *J. Chem. Phys.*, **71,** 4974.

27 Mountain R.D. and A.C. Brown (1984). *J. Chem. Phys.*, **80,** 2730.

28 Nosé S. and F. Yonezawa (1986). *J. Chem. Phys.*, **84,** 1803.

29 Yang J., Gould H., and W. Klein (1988). *Phys. Rev. Lett.*, **60,** 2665.

30 Swope W.C. and H.C. Andersen (1990). *Phys. Rev. B.*, **41,** 7042.

31 Bennett C.H. In A.S. Nowick and J.J. Burton, Eds., *Diffusion in solids: Recent developments,* pages 73-113. Academic press, New York, 1975, and *J. Comput. Phys.*, **22,** 245, 1976.

32 Chandler D. (1978). *J. Chem. Phys,* **68,** 2959, and D. Chandler (1987), *Introduction to Modern Statistical Mechanics.* Oxford University Press, New York.

33 Carter E.A., G. Ciccotti, J.T. Hynes, and R. Kapral (1989). *Chem. Phys. Lett.*, **156,** 472.

34 Ciccotti G. (1991), in *Computer Simulations in Materials Science,* edited by M. Meyer and V. Pontikis. Kluwer, Dordrecht, p. 119-137.

35 van Duijneveldt J.S. and D. Frenkel (1992). *J. Chem. Phys.*, **96,** 4655.

36 Torrie G.M. and J.P. Valleau (1974). *Chem. Phys. Lett.*, **28,** 578.

37 Steinhardt P.J., D.R. Nelson, and M. Ronchetti (1983). *Phys. Rev. B.*, **28,** 784.

38 Landau L.D. and E.M. Lifshitz (1980). *Statistical Physics,* 3rd ed., Pergamon, London.

39 P.R. ten Wolde, M.J. Ruiz-Montero, and D. Frenkel, in preparation.

Final manuscript received in November 1995